


# Nonlinear modes coupling of trapped spin-orbit coupled spin-1 Bose-Einstein condensates

Jie Wang(王杰), Jun-Cheng Liang(梁俊成), Zi-Fa Yu(鱼自发), An-Qing Zhang(张安庆), Ai-Xia Zhang(张爱霞), and Ju-Kui Xue(薛具奎)

**Citation:**Chin. Phys. B, 2023, 32 (**9**): 090305. DOI: 10.1088/1674-1056/accd53
Journal homepage: http://cpb.iphy.ac.cn; http://iopscience.iop.org/cpb

**What follows is a list of articles you may be interested in**

---

## Spin current in a spinor Bose-Einstein condensate induced by a gradient magnetic field

Li Tian(田丽), Ningxuan Zheng(郑宁宣), Jun Jian(蹇君), Wenliang Liu(刘文良), Jizhou Wu(武寄洲), Yuqing Li(李玉清), Yongming Fu(付永明), Peng Li(李鹏), Vladimir Sovkov, Jie Ma(马杰), Liantuan Xiao(肖连团), and Suotang Jia(贾锁堂)

Chin. Phys. B, 2022, 31 (**11**): 110302. DOI: 10.1088/1674-1056/ac80ac

## Dynamics of bright soliton in a spin-orbit coupled spin-1 Bose-Einstein condensate

Hui Guo(郭慧), Xu Qiu(邱旭), Yan Ma(马燕), Hai-Feng Jiang(姜海峰), and Xiao-Fei Zhang(张晓斐)

Chin. Phys. B, 2021, 30 (**6**): 060310. DOI: 10.1088/1674-1056/abf34a

## Ultradilute self-bound quantum droplets in Bose-Bose mixtures at finite temperature

Jia Wang(王佳), Xia-Ji Liu(刘夏姬), and Hui Hu(胡辉)

Chin. Phys. B, 2021, 30 (**1**): 010306. DOI: 10.1088/1674-1056/abd2ad

## Trapped Bose-Einstein condensates with quadrupole-quadrupole interactions

An-Bang Wang(王安邦), Su Yi(易俗)

Chin. Phys. B, 2018, 27 (**12**): 120307. DOI: 10.1088/1674-1056/27/12/120307

## High-fidelity quantum memory realized via Wigner crystals of polar molecules

Xue Peng(薛鹏) and Wu Jian-Zhi(午剑智)

Chin. Phys. B, 2012, 21 (**1**): 010308. DOI: 10.1088/1674-1056/21/1/010308

---

# Nonlinear modes coupling of trapped spin–orbit coupled spin-1 Bose–Einstein condensates

Jie Wang(王杰), Jun-Cheng Liang(梁俊成), Zi-Fa Yu(鱼自发), An-Qing Zhang(张安庆), Ai-Xia Zhang(张爱霞), and Ju-Kui Xue(薛具奎)†

*College of Physics and Electronics Engineering, Northwest Normal University, Lanzhou* 730070, *China*

(Received 11 January 2023; revised manuscript received 4 April 2023; accepted manuscript online 17 April 2023)

We study analytically and numerically the nonlinear collective dynamics of quasi-one-dimensional spin–orbit coupled spin-1 Bose–Einstein condensates trapped in harmonic potential. The ground state of the system is determined by minimizing the Lagrange density, and the coupled equations of motions for the center-of-mass coordinate of the condensate and its width are derived. Then, two low energy excitation modes in breathing dynamics and dipole dynamics are obtained analytically, and the mechanism of exciting the anharmonic collective dynamics is revealed explicitly. The coupling among spin–orbit coupling, Raman coupling and spin-dependent interaction results in multiple external collective modes, which leads to the anharmonic collective dynamics. The cooperative effect of spin momentum locking and spin-dependent interaction results in coupling of dipolar and breathing dynamics, which strongly depends on spin-dependent interaction and behaves distinct characters in different phases. Interestingly, in the absence of spin-dependent interaction, the breathing dynamics is decoupled from spin dynamics and the breathing dynamics is harmonic. Our results provide theoretical evidence for deep understanding of the ground sate phase transition and the nonlinear collective dynamics of the system.

**Keywords:** spin–orbit coupled spin-1 Bose–Einstein condenses, collective excitations, nonlinear modes coupling

**PACS:** 03.75.Mn, 03.75.Lm, 05.45.Yv **DOI:** 10.1088/1674-1056/accd53

## 1. Introduction

Ultra-cold atomic gases provide an ideal platform for exploring novel spin–orbit (SO) coupling physics, owing to their unprecedented levels of control[1–4] and precision in experiments. In ultra cold atomic gases, SO coupling can be generated by the two-photon Raman coupling technique.[5–9] Recently, SO-coupled spin-1 Bose–Einstein condensates (BECs) have been successfully achieved in experiments through Raman coupling among three hyperfine states of atoms,[2,10] thus paving the way to explore the rich physics of SO-coupled spin-1 BECs. Theoretical predictions and experimental observations of SO-coupled spin-1 BECs render various novel ground-state phases including plane wave phase, stripe phase and zero-momentum phases, etc.[11–14]

The collective excitation also provides an effective tool for exploring the physics of the condensates, and can be used to identify the phase transition of the system dynamically. The collective excitation of the spin-1/2 BECs with SO coupling has been widely and deeply explored experimentally[7,15] and theoretically[16,17] by using the sum rule approach[18] and the Bogoliubov spectrum analysis.[19] It is found that the collective dynamics is trivial for conventional condensates and the collective oscillation is harmonic.[20,21] However, the collective dynamics of the trapped spinor BECs is complex. Meanwhile, because of emergence of nonlinearity, a lot of interesting phenomena in the collective excitations of BECs, such as frequency shift,[22] mode coupling,[23–25] damping,[26,27] collapse and revival of oscillations,[28,29] are observed.

Recently, elementary excitations of SO-coupled spin-1 Boses gases are studied in free space, and it is found that phonon modes of different phases have different structures of rotons.[12,13,30] Noticeably, in trapped SO coupling spin-1 cold-atomic systems, an analogy of Hall response can be detected through collective excitations.[31] In Ref. [32], the collective excitation of a quasi-one-dimensional SO-coupled spin-1 BEC at finite temperatures for antiferromagnetic spin interactions was studied by utilizing the Hartree–Fock–Bogolyubor–Popov approximation. Moreover, the spin dynamics of spin-1 condensates in an external magnetic field is studied,[33] which exhibits a variety of periodic oscillations and provides theoretical support for interactions-driven oscillations. In general, because of coupling effects (induced by SO coupling and Raman coupling) and strong nonlinearity (induced by density-dependent interaction and spin-dependent interaction), rich nonlinear modes coupling (harmonic, anharmonic and irregular dynamics) should exist in SO-coupled spin-1 BECs. Accordingly, the nonlinear modes coupling will result in rich nonlinear spin dynamics. However, those are still open subjects. Particularly, the physical mechanism of generating anharmonic collective dynamics and the transition of harmonic-anharmonic dynamics in different phases of the system are still unclear.

In this paper, we study collective dynamics of SO-coupled spin-1 BECs in harmonic potential bath analytically

†Corresponding author. E-mail: xuejk@nwnu.edu.cn

© 2023 Chinese Physical Society and IOP Publishing Ltd 

and numerically. Using variational approaches, the coupled equations of motions for the center-of-mass coordinate of the condensate and its width are derived. Then, two low energy excitation modes in breathing dynamics and dipole dynamics are obtained analytically, which are in agreement with the numerical results of solving the Gross–Pitaevskii equation. We find that the dipolar dynamics for center-of-mass motion and the breathing dynamics for width variation of condensate are coupled through the spin dynamics induced by the SO coupling. This leads to the emergence of multiple external collective modes. Thus, the dipolar and breathing oscillation will be the superposition of the multiple harmonic oscillations, which generates an anharmonic collective dynamics. Furthermore, in anharmonic oscillations, breathing oscillations can be induced by excited dipole oscillations, and vice versa. Interestingly, spin-dependent interactions play an important role in collective excitation. In dipole dynamics, two degenerate low-energy excitation modes become non-degenerate as spin-dependent interaction increases. In breathing dynamics, however, when spin-dependent interaction is absent, the breathing dynamics is decoupled from spin dynamics and dipole dynamics, in which the breathing oscillation is harmonic. Particularly, we find that the collective dynamics is distinct in different phases, which is revealed both analytically and numerically.

The paper is organized as follows. In Section 2, based on the mean field approximation, we obtain the Hamiltonian of SO-coupled spin-1 BECs in a quasi-one-dimensional harmonic potential. In Sections 3 and 4, the variational equation of the system is obtained by minimizing the Lagrange density and the ground state phase of the system is analyzed in detail. In Sections 5, two low energy excitation modes in dipole dynamics and breathing dynamics are obtained analytically and verified numerically. Then the physical mechanism causing the anharmonic oscillation is discussed and the coupling effect of spin dynamics and breathing dynamics is emphasized, which leads to the phenomenon that the dipole (breathing) mode induces the breathing (dipole) mode in anharmonic oscillation. Finally in Section 6 we present conclusions.

## 2. The model

We study the collective dynamics of SO-coupled spin-1 BECs in harmonic potential. The SO coupling is characterized by equally weighted Rashba and Dresselhaus SO coupling.[7] The SO coupling only exists in the $\hat{x}$ direction and mainly affects the collective dynamics in the $\hat{x}$ direction, while the dipole oscillations in the $\hat{y}$ and $\hat{z}$ directions are still harmonic oscillations, and the oscillation frequency is the harmonic potential frequency in that direction. Furthermore, when the strength of the trapping potential in the $\hat{y}$ and $\hat{z}$ directions is much larger than the frequency of the trapping potential in the $\hat{x}$ direction, the transverse degrees of freedom of the system are frozen such that the dynamics of the system only occurs in the $\hat{x}$ direction. Therefore, we consider the one-dimensional case and discuss the nonlinear mode coupling caused by SO coupling in the $\hat{x}$ direction. According to the recent experiments[34,35] about the realization of SO-coupled spin-1 BECs, the dynamics of the BECs trapped in harmonic trap can be expressed by a dimensionless mean-field Gross–Pitaevskii equation (GPE) for normalized spinor wave function $\Psi = (\psi_1, \psi_0, \psi_{-1})^{\mathrm{T}}$ as[13,36]

$$\mathrm{i}\partial_t \Psi(\boldsymbol{x},t) = (h_0 + 2h_{\mathrm{int}})\Psi(\boldsymbol{x},t), \tag{1}$$

where $h_0 = -\frac{1}{2}\partial_x^2 + \mathrm{i}2\gamma\partial_x F_z + (\Delta + 2\gamma^2)F_z^2 + \sqrt{2}\Omega F_x + V_{\mathrm{ext}}$ is the dimensionless single-particle Hamiltonian. Here, $\boldsymbol{F} = (F_x, F_y, F_z)$ is the spin-1 operator; $\gamma = l_\perp k_{\mathrm{R}}$ is the dimensionless SO coupling strength, $k_{\mathrm{R}} = \frac{2\pi}{\lambda_{\mathrm{R}}}$ with $\lambda_{\mathrm{R}}$ being the wavelength of Raman lasers. $\Omega = \tilde{\Omega}/(\hbar\omega_\perp)$ is the dimensionless Raman coupling (RC) strength; $\Delta = \tilde{\Delta}/(\hbar\omega_\perp)$ is the dimensionless quadratic Zeeman strength; $l_\perp = \sqrt{\hbar/(m\omega_\perp)}$ is the transverse characteristic length of the condensates with external trapping frequency $\omega_\perp$, with $m$ being the atomic mass. $V_{\mathrm{ext}} = \frac{1}{2}\omega^2 x^2$ is the external harmonic potential along $\hat{x}$ direction with $\omega = \omega_x/\omega_\perp$ ($\omega_\perp \gg \omega_x$). In addition, the dimensionless interatomic two-body interaction can be written as[12,37] $h_{\mathrm{int}} = \frac{g_0}{2}(\Psi^\dagger\Psi) + \frac{g_2}{2}(\Psi^\dagger \boldsymbol{F}^2\Psi)$, where density-dependent interaction $g_0 = 2N\hbar(a_0 + 2a_2)/(3m\omega_\perp l_\perp^3)$ and spin-dependent interaction $g_2 = 2N\hbar(a_2 - a_0)/(3m\omega_\perp l_\perp^3)$ are related to the s-wave scattering lengths, with $N$ being the total number of atoms.[38–41] The detailed dimension reduction process and dimensionless process are dipicted in Appendix A. In the experiment, $g_0$ and $g_2$ could also be tuned through Feshbach resonances.[42]

## 3. The variational analysis

Now, the selection of the proper form of the trial functions is crucial. In our case, a natural choice is a Gaussian, i.e., we take

$$\Psi = \begin{pmatrix} \psi_1 \\ \psi_0 \\ \psi_{-1} \end{pmatrix} = \begin{pmatrix} \frac{\mathrm{e}^{\mathrm{i}(\alpha+\beta)/2}}{\sqrt{2}}\sqrt{m_z + M} \\ -\sqrt{1 - m_z} \\ \frac{\mathrm{e}^{\mathrm{i}(\alpha-\beta)/2}}{\sqrt{2}}\sqrt{m_z - M} \end{pmatrix} \varphi(x), \tag{2}$$

where $\varphi(x)$ is a normalized Gaussian function

$$\varphi(x) = \frac{\exp\left[-\frac{(x-x_0)^2}{2R^2} + \mathrm{i}k(x-x_0) + \frac{\mathrm{i}}{2}\delta(x-x_0)^2\right]}{(\sqrt{\pi}R)^{1/2}} \tag{3}$$

with the width $R$, the center-of-mass position $x_0$, momentum $k$ along $\hat{x}$ direction and the variational rate of radius $\delta$ of the wave packets. Here, $\alpha$ and $\beta$ are variational parameters of the related phases of the two spin states. In particular, the average spin polarization $\langle F_z\rangle = M = \int(|\psi_1|^2 - |\psi_{-1}|^2)\mathrm{d}x$ and spin tensor $\langle F_z^2\rangle = m_z = \int(|\psi_1|^2 + |\psi_{-1}|^2)\mathrm{d}x$

can be measured in experiment. Notice that the parameters $(R,k,\delta,\alpha,\beta,x_0,M,m_z)$ are all time dependent. The nonlinear dynamics is controlled by a set of coupled Gross–Pitaevskii equations. However, the problem of solving the Gross–Pitaevskii equations can be formulated as a variational problem that minimizes the Lagrangian density. Upon substitute the spinor wave function into the Lagrangian $\pounds = \int[(\mathrm{i}/2)(\Psi^*\dot{\Psi}-\Psi\dot{\Psi}^*)-\Psi^*(h_0+h_{\mathrm{int}})\Psi]\mathrm{d}x$, one can obtain

$$\pounds = k\dot{x}_0 - M\dot{\alpha} - \frac{1}{4}R^2\dot{\delta} - m_z\dot{\beta} - E, \tag{4}$$

where

$$\begin{aligned} E =& \frac{1}{2}k^2 - 2\gamma kM + \frac{1}{4}\omega^2(R^2+2x_0^2) + \frac{1}{4R^2} + \frac{1}{4}R^2\delta^2 \\ &+ (2\gamma^2+\Delta)m_z - \Omega\cos(\alpha-\beta)(m_z-M) \\ &- \Omega\cos(\alpha+\beta)\sqrt{m_z^2-M^2} + \frac{g_0+g_2M^2}{2\sqrt{2\pi}R} \\ &- \frac{2g_2(m_z-1)(m_z+\cos(2\beta)\sqrt{m_z^2-M^2})}{2\sqrt{2\pi}R}. \end{aligned} \tag{5}$$

Applying the Euler–Lagrangian equations $\partial\pounds/\partial q_i - \mathrm{d}(\partial\pounds/\partial\dot{q}_i)/\mathrm{d}t = 0$, where $q_i = \{k,R,M,m_z,x_0,\alpha,\beta,\delta\}$, we arrive at

$$\dot{k} = -\omega^2 x_0, \tag{6}$$

$$\dot{x}_0 = k - 2\gamma M, \tag{7}$$

$$\dot{R} = R\delta, \tag{8}$$

$$\begin{aligned} \dot{\delta} =& \frac{2g_2(1-m_z)(m_z+\cos(2\beta)\sqrt{m_z^2-M^2})}{\sqrt{2\pi}R^3} \\ &- \omega^2 + \frac{1}{R^4} + \frac{g_0+g_2M^2}{\sqrt{2\pi}R^3}, \end{aligned} \tag{9}$$

$$\begin{aligned} \dot{M} =& \Omega\sqrt{2-2m_z}\big[\sqrt{m_z-M}\sin(\alpha-\beta) \\ &+ \sqrt{m_z+M}\sin(\alpha+\beta)\big], \end{aligned} \tag{10}$$

$$\begin{aligned} \dot{m}_z =& \frac{\sqrt{2}g_2\sqrt{m_z^2-M^2}\sin(2\beta)}{\sqrt{\pi}R}(m_z-1) \\ &+ \Omega\sqrt{2-2m_z}\big[\sqrt{m_z+M}\sin(\alpha+\beta) \\ &- \sqrt{m_z-M}\sin(\alpha-\beta)\big], \end{aligned} \tag{11}$$

$$\begin{aligned} \dot{\alpha} =& 2\gamma k + \frac{1}{2}\Omega\sqrt{2-2m_z}\Big(-\frac{\cos(\alpha-\beta)}{\sqrt{m_z-M}} + \frac{\cos(\alpha+\beta)}{\sqrt{m_z+M}}\Big) \\ &- \frac{g_2M\big[\sqrt{m_z^2-M^2}+\cos(2\beta)(m_z-1)\big]}{\sqrt{2\pi}R\sqrt{m_z^2-M^2}}, \end{aligned} \tag{12}$$

$$\begin{aligned} \dot{\beta} =& -(2\gamma^2+\Delta) + \frac{g_2\cos(2\beta)M^2}{\sqrt{2\pi}R\sqrt{m_z^2-M^2}} \\ &+ \frac{g_2\big[(1-2m_z)(\cos(2\beta)m_z+\sqrt{m_z^2-M^2})\big]}{\sqrt{2\pi}R\sqrt{m_z^2-M^2}} \\ &+ \frac{1}{2}\Omega\sqrt{2-2m_z}\Big(\frac{\cos(\alpha-\beta)}{\sqrt{m_z-M}} + \frac{\cos(\alpha+\beta)}{\sqrt{m_z+M}}\Big) \\ &- \frac{\Omega\big[\cos(\alpha-\beta)\sqrt{m_z-M}+\cos(\alpha+\beta)\sqrt{m_z+M}\big]}{\sqrt{2-2m_z}}. \end{aligned} \tag{13}$$

Equations (6)–(9) describe the wave packet dynamics of the system, while Eqs. (10)–(13) give the spin dynamics of the system. It is clear that, because of spin-momentum locking and spin-dependent interaction [Eqs. (7), (10), and (11)], the wave packet dynamics and the spin dynamics are coupled. As discussed in the following sections, the ground state and the dynamics of the system are well described by the Eqs. (6)–(13). The variational analysis with Gaussian ansatz is widely used in studying the dynamics of trapped interacting Bose gas. In literature,[43,44] an intensive study of the reasonability of Gaussian ansatz and variational method was also provided. The reasonability of our variational results obtained with Gaussian ansatz (3) is further well confirmed by numerical simulations of the full GPE (1).

## 4. The ground state

The ground state of the system can be obtained by solving the equations of steady state, i.e., $\dot{q}_i = 0$. We find the SO coupled BECs condensate into the momentum state $k = k_{\mathrm{min}} = 2\gamma M$. Thus, the ground state phases of the system can be determined by the order parameter $M$. When $M = 0$, the condensates are in zero momentum state. On the contrary, when $M \neq 0$, the condensates are in nonzero momentum state. In addition, by substituting the solutions of the steady state equations into Eq. (5), we can numerically obtain the ground state energy of the system. Then, the ground states of the system can be determined.

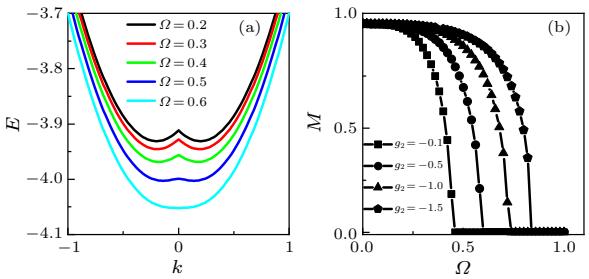



**Fig. 1.** (a) The energy band of the system as a function of $k$ for different $\Omega$ with $g_2 = -0.5$. (b) The average spin polarization $|M|$ against $\Omega$ for different $g_2$. We set $g_0 = 1$, $\gamma = 0.1$, $\omega = 0.1$, and $\Delta = -4$.

To identify the ground state phases of the system, we plot the energy band structure and average spin polarization $|M|$ with different $\Omega$ in Fig. 1. It is obvious that, with $\Omega$ increasing, the spin polarization $M$ decreases from a finite value to zero and the band structure changes from a double degenerate minimum with $k \neq 0$ to a single degenerate minimum with $k = 0$. This proves that the system has undergone a phase transition. For $M \neq 0$, the atoms condense in the $k = \pm 2\gamma M$ state, the energy band structure has a double well structure.

In this case, there are different numbers of atoms in the two spin states $m_F = 1$ and $m_F = -1$, thus the condensates are in a magnetized state (spin polarized state) with nonzero momentum. For $M = 0$, the atoms condense in the zero momentum state, and the band structure presents a parabolic structure. In this case, the two spin states $m_F = \pm 1$ have the same number of atoms, thus the condensates are in an unmagnetized state with zero momentum.

## 5. The collective excitation

To analyze the dipolar and breather modes, we consider the weak perturbation around the equilibrium state $q_{i0}$ of Eqs. (6)–(13). Substituting $q_i = q_{i0} + \delta q_i$ into Eqs. (6)–(13), the linearized equations for collective dynamics are acquired as follows:

$$\delta\ddot{x}_0 + \omega^2\delta x_0 + 2\gamma\delta\dot{M} = 0, \tag{14}$$

$$\delta\ddot{M} - A_0\delta\dot{x}_0 - A_1\delta R - A_2\delta M - A_3\delta m_z = 0, \tag{15}$$

$$\delta\ddot{m}_z - B_0\delta\dot{x}_0 - B_1\delta R - B_2\delta M - B_3\delta m_z = 0, \tag{16}$$

$$\delta\ddot{R} + C_1\delta R - C_2\delta M - C_3\delta m_z = 0, \tag{17}$$

where $A_0 = 2a_1\gamma$, $A_1 = a_0a_6 + a_1a_3$, $A_2 = a_0a_8 + a_1(-4\gamma^2 + a_4)$, $A_3 = a_0a_7 + a_1a_5$, $B_0 = 2a_0\gamma$, $B_1 = a_0a_3 + (a_1 + a_2)a_6$, $B_2 = a_0(-2\gamma^2 + a_4) + (a_1 + a_2)a_8$, and $B_3 = a_0a_5 + (a_1 + a_2)a_7$. The coefficients $a_i (i = 0 - 8)$ and $C_j$ $(j = 1, 2, 3)$ are given in Appendix B. Owing to the SO coupling, there is a coupling between dipolar and breathing dynamics through spin dynamics. Thus, the collective oscillations can be regarded as the superposition of the four collective modes in general cases, which leads to the emergence of the anharmonic collective behaviors.

### 5.1. Dipolar dynamics

Firstly, we only focus on the dipolar oscillation, and assume that the width of condensate still remains unchanged under the weak excitation, i.e., $\delta R = 0$. Based on Eqs. (14)–(16), one can obtain

$$\delta x_0^{(6)} + D_{11}\delta x_0^{(4)} + D_{12}\delta x_0^{(2)} + D_{13} = 0, \tag{18}$$

where $D_{11} = -A_2 - B_3 + 2A_0\gamma + \omega^2$, $D_{12} = B_3A_2 - A_2\omega^2 - A_3B_2 + 2A_3B_0\gamma - B_3\omega^2$, $D_{13} = A_2B_3\omega^2 - A_3B_2\omega^2$; $\delta x_0^{(n)}$ is the $n$-th order derivative of $\delta x_0$ about $t$. From the characteristic equation (18), the low-frequency mode $\omega_{DL}$ and the high-frequency mode $\omega_{DH}$ of the dipolar oscillation can be acquired as follows:

$$\omega_{DL,H} = \frac{1}{2\sqrt{3A^{1/3}}}[\pm 2^{4/3}D_{11}^2 + 6\times 2^{1/3}D_{12} + 2D_{11}A^{1/3} - (2A)^{2/3}]^{1/2}, \tag{19}$$

where

$$A = 2D_{11}^2 - 9D_{11}D_{12} + 27D_{13} + 3\sqrt{3}(-D_{11}^2D_{12}^2 + 4D_{12}^3 + 4D_{11}^3D_{13} - 18D_{11}D_{12}D_{13} + 27D_{13}^3)^{1/2}, \tag{20}$$

and the dipolar oscillation can be described by

$$x_0 = A_{DL}\cos(\omega_{DL}t) + A_{DH}\cos(\omega_{DH}t), \tag{21}$$

$$A_{DL} = \frac{\omega^2 - \omega_{DH}^2}{\omega_{DL}^2 - \omega_{DH}^2}\delta x_0, \tag{22a}$$

$$A_{DH} = \frac{\omega_{DL}^2 - \omega^2}{\omega_{DL}^2 - \omega_{DH}^2}\delta x_0, \tag{22b}$$

with $\delta x_0$ being the initial deviation of the center-of-mass from the equilibrium position.

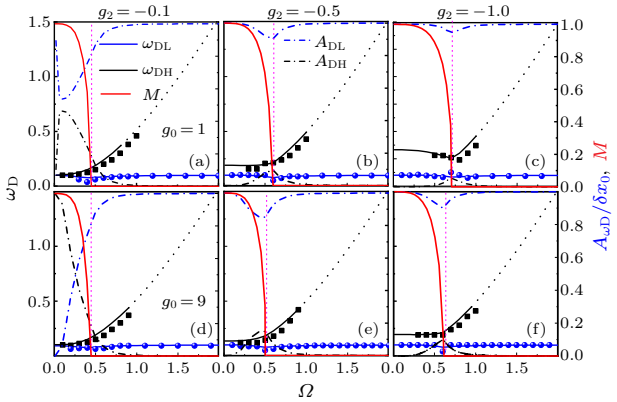



**Fig. 2.** Frequency and the corresponding amplitude of the dipolar oscillation versus $\Omega$ for different $g_0$ and $g_2$, where $\gamma = 0.1$, $\Delta = -4$, and $\omega = 0.1$: (a)–(c) for $g_0 = 1$, (d)–(e) for $g_0 = 9$. The corresponding $M$ in the ground state is represented by the solid red line, the dashed black line is the higher-frequency mode with zero amplitude. The results of direct numerical simulation of GPE (1) is represented by symbols. The red dashed line marks the phase transition point.

For a conventional condensate, the dipolar oscillation is trivial, its frequency is just the harmonic-trap frequency and is independent of SO coupling, RC and inter-atomic interactions. However, for an SO coupled condensate, the dipolar-oscillation frequency is different from the trapping frequency. The coupling effect of SO coupling, RC and atomic interactions is generation of two external dipolar modes, which can lead to the dipolar dynamics in the superposition of the two harmonic oscillations. When one of the two external frequencies is the inherent frequency, and the amplitude of the other external frequency vanishes, the dipolar oscillation is harmonic, otherwise it is the anharmonic dipolar oscillation. Whether the dipolar oscillation is harmonic depends on the competition between the two external modes, this is demonstrated in Eqs. (21) and (22) and clearly shown in Fig. 2. In Fig. 2, the phase transition point $\Omega = \Omega_c$ is represented by $M = 0$. When $\Omega = 0$ and $|g_2|$ is small [see Figs. 2(a) and 2(d)], the two modes degenerate to the trapping frequency, i.e., $\omega_{DL} = \omega_{DH} = \omega$. With the increase of $|g_2|$, the two degeneracy frequencies are split apart, and the larger the $|g_2|$ is, the more obvious the split is. However, the larger $g_0$ weakens the effect of $g_2$ on $\omega_{DH}$ [see Figs. 2(d)–2(f)]. As shown in Fig. 2, the

lower-frequency mode $\omega_{\rm DL}$ does not change much and keeps at trapping frequency as $\Omega$ increases, i.e., $\omega_{\rm DL} \cong \omega$, whereas the higher-frequency mode $\omega_{\rm DH}$ always increases with $\Omega$, especially in the $\Omega > \Omega_{\rm c}$ region. When the system is deeply in the unmagnetized phase ($\Omega \gg \Omega_{\rm c}$), the dipolar oscillation is harmonic with $\omega_{\rm DL} = \omega$ ($A_{\rm DL} = 1$ and $A_{\rm DH} = 0$). However, around the phase transition point ($\Omega \approx \Omega_{\rm c}$), the collective excitation of the system is complicated and anharmonic. In this case, many modes will be excited. When the system is in the fully magnetized phase ($\Omega \ll \Omega_{\rm c}$), the amplitude $A_{\rm DH}$ corresponding to mode $\omega_{\rm DH}$ disappears and the dipolar oscillation is also harmonic with $\omega_{\rm DL} = \omega$. In this case, $M \to 1$ and $m_z \to 1$, nearly all atoms condense in the spin state of $m_{\rm f} = 1$ (i.e. $|\Psi_{-1}|^2 \to 0$, $|\Psi_0|^2 \to 0$ and $|\Psi_1|^2 \to 1$), it can be approximated that the system is nearly one-component, spin dynamics disappears, so dipolar oscillation is harmonic.

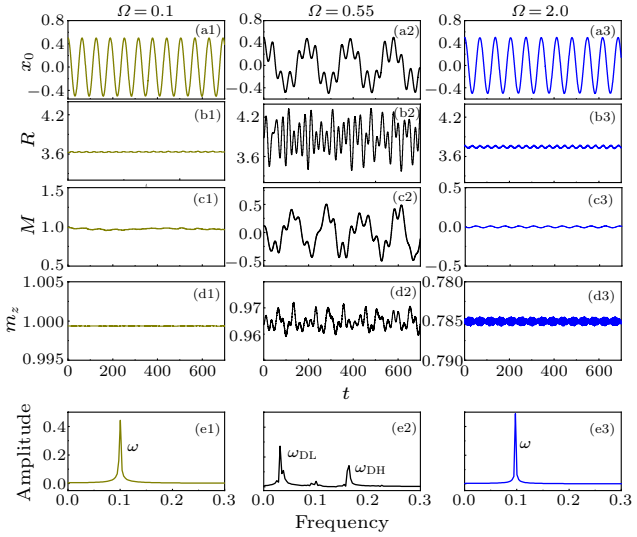



**Fig. 3.** The dipolar dynamics started in the fully magnetized phase with $\Omega = 0.1$ (a1)–(e1), in the magnetized phase near phase transition point with $\Omega = 0.55$ (a2)–(e2), and in the deep unmagnetized phase with $\Omega = 2.0$ (a3)–(e3). (e1)–(e3) The corresponding spectrum analyses of dipolar oscillation. We set $\gamma = 0.1$, $g_0 = 1$, $g_2 = -0.5$, $\delta x_0 = 0.5$, $\delta R = 0$, $\omega = 0.1$, and $\Delta = -4$.

To confirm the variational prediction, with small displacement of the center mass position of wave packets from the ground state, we perform direct numerical simulations of full GPE (1) using the fourth-order Runge–Kutta method, and the dipolar dynamics in the different phase regions is depicted in Fig. 3. Meanwhile, the numerical results of the two dipolar modes are also shown in Fig. 2, we find that the variational results are in good agreement with the numerical simulations. When the condensates are perturbed in nearly fully magnetized phase [see Figs. 3(a1)–3(e1)], as predicted by variational analysis [see Fig. 2], the amplitude of higher-frequency mode $A_{\rm DH}$ is zero, the dipolar oscillating is harmonic with $\omega_{\rm DL} = \omega$ [see Fig. 3(e1)]. In this case, $M \to 1$ and $m_z \to 1$ [see Figs. 3(c1)–3(d1)], the spin dynamics disappears, the breathing dynamics cannot be excited, $R \approx R_0$ [see Fig. 3(b1)]. When the condensates are excited in a magnetized phase near the phase transition point [see Figs. 3(a2)–3(e2)], where the dipolar dynamics and the breathing dynamics are strongly coupled due to SO coupling [see Eqs. (14)–(17)], the dipolar oscillation is anharmonic and its oscillation frequency is the superposition of two modes $\omega_{\rm DL}$ and $\omega_{\rm DH}$ [see spectrum analysis in Fig. 3(e2)]. In addition, the dipolar dynamics induces complex and irregular breathing dynamics and spin dynamics [see Figs. 3(b2)–3(d2)]. When the condensates are excited in the deep unmagnetized phase [see Figs. 3(a3)–3(e3)], where the dipolar dynamics and the breathing dynamics are decoupled due to $M = 0$ [see Eqs. (14)–(17)], the dipolar oscillating is harmonic, the dipolar dynamics cannot induce the breathing dynamics and spin dynamics [see Figs. 3(b3) and 3(d3)].

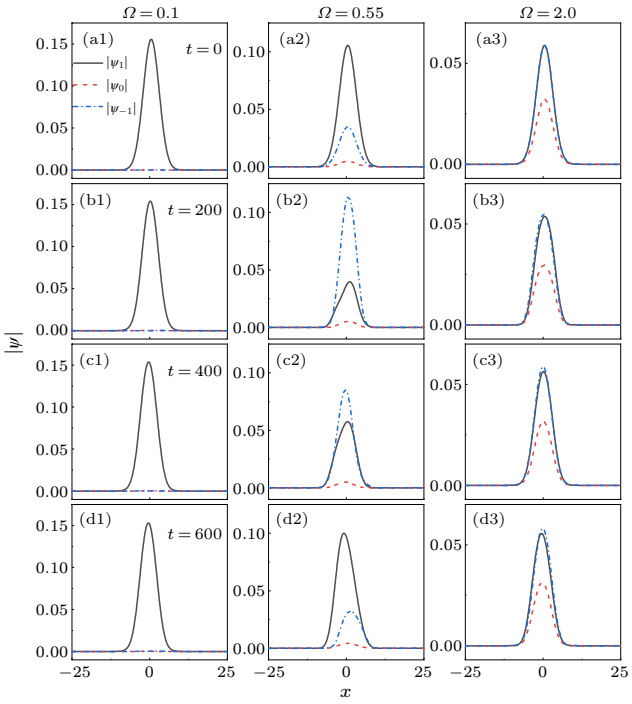



**Fig. 4.** Time evolution of the three pseudo spin states $|\psi_1|$, $|\psi_0|$ and $|\psi_{-1}|$ in the fully magnetized phase with $\Omega = 0.1$ (the first column), in the unmagnetized phase near phase transition point with $\Omega = 0.55$ (the second column) and in the deep magnetized phase with $\Omega = 2.0$ (the third column). We set $g_0 = 1$, $g_2 = -0.5$, $\gamma = 0.1$, $\omega = 0.1$, and $\Delta = -4$.

The corresponding wave packets in different ground state phases are shown in Fig. 4. The wave packets $|\psi_1|$, $|\psi_0|$ and $|\psi_{-1}|$ are always Gaussian like. In the case of full magnetized phase [see Figs. 4(a1)–4(d1)], $M \to 1$, $m_z \to 1$, only one component $|\psi_1|$ exists and there is almost no spin exchange between the spin components $|\psi_1|$ and $|\psi_{-1}|$. However, in the magnetized phase near phase transition point, the dynamic behaviors of two pseudo spin components $|\psi_1|$ and $|\psi_{-1}|$ are different [see Figs. 4(a2)–4(d2)], the strong spin exchange can be observed evidently. In addition, $|\psi_1|$ and $|\psi_{-1}|$ are almost coincided in the deep unmagnetized phase [see Figs. 4(a3)–4(d3)], $M = 0$, the spin exchange between two pseudo spin components is very weak in this case. We conclude that strong

spin dynamic induces strong coupling of dipolar and breather modes, which results in anharmonic and complex wave packets dynamics and spin dynamics. The numerical simulation confirm the variational predictions.

### 5.2. Breathing dynamics

When considering the breathing dynamics under the weak excitation, the mass center of condensates can be regarded to be at rest, i.e., $\delta x_0 = 0$. Based on Eqs. (15)–(17), one can obtain

$$\delta R^{(6)} - D_{21}\delta R^{(4)} + D_{22}\delta R^{(2)} + D_{23} = 0, \tag{23}$$

where $D_{21} = -(A_2+B_3+C_1)$, $D_{22} = -A_1C_2 - A_3B_2 + A_2B_3 + A_2C_1 + B_3C_1 - B_1C_3$, $D_{23} = A_1B_3C_2 - A_1B_2C_3 + A_3B_2C_1 - A_2B_3C_1 - A_3B_1C_2 + A_2B_1C_3$; $\delta R^{(n)}$ is the $n$-th order derivative of $\delta R$ about $t$. From Eq. (23), the low-frequency mode $\omega_{\rm BL}$ and the high-frequency mode $\omega_{\rm BH}$ of the breathing oscillation can be acquired as follows:

$$\omega_{\rm BL,H} = \frac{1}{2\sqrt{3}B^{1/3}}[\pm 2^{4/3}D_{21}^2 + 6\times 2^{1/3}D_{22} + 2D_{21}B^{1/3} - (2B)^{2/3}]^{1/2}, \tag{24}$$

where

$$B = 2D_{21}^2 - 9D_{21}D_{22} + 27D_{23} + 3\sqrt{3}(-D_{21}^2D_{22}^2 + 4D_{22}^3 + 4D_{21}^3D_{23} - 18D_{21}D_{22}D_{23} + 27D_{23}^3)^{1/2}. \tag{25}$$

The breathing oscillation can be described by

$$R = R_0 + A_{\rm BL}\cos(\omega_{\rm BL}t) + A_{\rm BH}\cos(\omega_{\rm BH}t), \tag{26}$$

where

$$A_{\rm BL} = \frac{C_1 - \omega_{\rm BH}^2}{\omega_{\rm BL}^2 - \omega_{\rm BH}^2}\delta R, \tag{27a}$$

$$A_{\rm BH} = \frac{\omega_{\rm BL}^2 - C_1}{\omega_{\rm BL}^2 - \omega_{\rm BH}^2}\delta R, \tag{27b}$$

with $\delta R = R - R_0$ being the deviation of width from $R_0$ initially.

The inherent frequency of the breathing oscillation for a conventional condensate is $\omega_{\rm B0} = \sqrt{C_1} = \sqrt{3\omega^2 + 1/R_0^4}$, which depends on the harmonic trapping and atomic interactions. However, the breather modes are complex for spinor BECs, which is related to SO coupling, RC, harmonic trapping, and atomic interactions. Obviously, under a weak excitation, the breathing dynamics of trapped BECs with SO coupling is also the superposition of the two harmonic oscillations with frequencies $\omega_{\rm BL}$ and $\omega_{\rm BH}$. The competition of the two breather modes is clearly depicted in Fig. 5.

Similar to dipolar dynamics, when one of the two external frequencies is the inherent frequency, and the amplitudes of the other external frequencies vanish [see Eqs. (27a) and (27b)], the breathing oscillation is harmonic, otherwise it is anharmonic. Whether the breathing oscillation is harmonic depends on the competition between the two external modes, which is demonstrated in Eqs. (26) and (27). In addition, the spin-dependent interaction $g_2$ has an important effect on breathing dynamics. In particular, when $g_2 = 0$, breathing dynamics is decoupled not only from spin dynamics but also from dipolar dynamics due to coefficients $C_2 = 0$ and $C_3 = 0$ [see Eq. (17) or Eqs. (8) and (9)]. In this case, the breathing oscillation is also harmonic with $\omega_{\rm B0}$. Meanwhile, different from the dipolar mode, the two breather modes do not degenerate when $g_2$ is small and $g_2$ only has a greater influence on $\omega_{\rm BH}$ mode. However, the larger $g_0$ weakens the effect of $g_2$ on $\omega_{\rm DH}$ [see Figs. 5(d)–5(f)]. As shown in Fig. 5, the lower-frequency mode $\omega_{\rm BL}$ always varies around the inherent frequency $\omega_{\rm B0} = \sqrt{C_1}$ as $\Omega$ increases. Contrarily, the higher-frequency mode $\omega_{\rm BH}$ always increases with $\Omega$, especially in the $\Omega > \Omega_{\rm c}$ region. When the system is in the fully magnetized phase ($\Omega \ll \Omega_{\rm c}$), $M \to 1$, $m_z \to 1$, spin dynamics disappears, the breathing dynamics is harmonic with high-frequency mode $\omega_{\rm BH}$. The breathing dynamics around the phase transition point ($\Omega \approx \Omega_{\rm c}$) is also complex for the reasons similar to that of the dipolar mode, i.e., strong coupling of breathing dynamics and spin dynamics occurs. However, when the system is deeply in the unmagnetized phase ($\Omega \gg \Omega_{\rm c}$), $M = 0$, the spin and breathing dynamics are decoupled, the breathing oscillation is also harmonic with $\omega_{\rm BL} \cong \omega_{\rm B0}$ ($A_{\rm BL} = 1$ and $A_{\rm BH} = 0$).

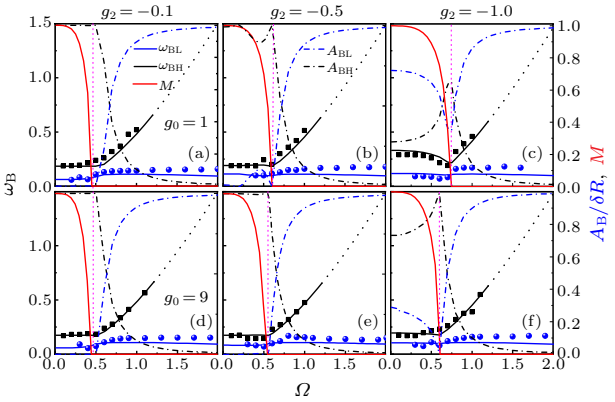



**Fig. 5.** The same as Fig. 2 but for the breathing oscillation.

To prove the variational predictions, with the weak perturbation of wave packet width from the ground state, the breathing dynamic behaviors of different phase regions are obtained by numerical simulation [see Fig. 6]. Meanwhile, the numerical simulation results of the two breather modes are also shown in Fig. 5. We find that variational results are also in good agreement with the numerical simulations. When the condensates are disturbed in nearly fully magnetized phase [Figs. 6(a1)–6(e1)], as predicted by variational analysis [Fig. 5], the amplitude of lower-frequency mode $\omega_{\rm BL}$ is zero, and the breathing oscillation is harmonic with $\omega_{\rm BH}$. In

this case, the dipolar dynamics and spin dynamics are not excited [see Figs. 6(b1)–6(e1)]. When the condensates are excited in a magnetized phase around the phase transition point, the breathing oscillation is anharmonic [see Fig. 6(a2)] due to dipolar dynamics and spin dynamic behaviors are excited [see Figs. 6(b2) and 6(c2)]. At the same time, breathing oscillation frequency is the superposition of two frequencies $\omega_{\rm BL}$ and $\omega_{\rm BH}$ [see spectrum analysis in Fig. 6(e2)]. When the condensates are excited in the deep unmagnetized phase [see Figs. 6(a3)–6(e3)], where the breathing dynamics and the dipolar dynamics are decoupled due to $M = 0$ [see Eqs. (14)–(17)], the breathing oscillation is harmonic, and the breathing dynamics cannot induce the dipolar dynamics and spin dynamics [see Figs. 6(b3)–6(e3)]. Interestingly, in this case, although the spin tensor $m_z$ is excited, it has weak effect on the collective dynamic of the system.

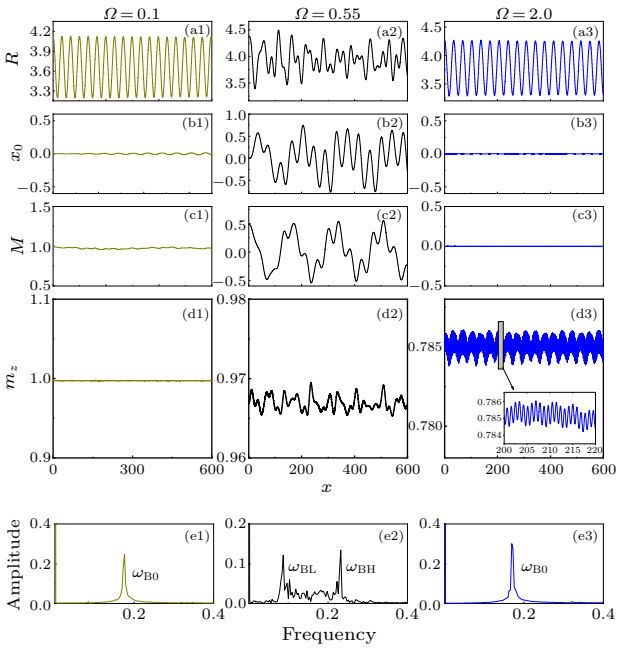



**Fig. 6.** Breathing dynamics started in the fully magnetized phase with $\Omega = 0.1$ (a1)–(e1), in the magnetized phase near phase transition point with $\Omega = 0.55$ (a2)–(e2), and in the deep unmagnetized phase with $\Omega = 2.0$ (a3)–(e3). (e1)–(e3) The corresponding spectrum analyses of breathing oscillation. We set $g_0 = 1$, $g_2 = -0.5$, $\gamma = 0.1$, $\delta R = 0.5$, $\delta x_0 = 0$, $\omega = 0.1$, and $\Delta = -4$. The inset in (d3) is a larger view of the gray area.

In breathing dynamics, the corresponding wave packets dynamics in different ground state phases are shown in Fig. 7. In the fully magnetized phase [Figs. 7(a1)–7(d1)], $M \to 1$, $m_z \to 1$, the condensates keep in the $m_{\rm F} = 1$ state during the breathing dynamics. The numerical results well confirm the variational predictions. In the magnetized phase near phase transition point [Figs. 7(a2)–7(d2)], the wave packets of the two spin components $|\psi_1|$ and $|\psi_{-1}|$ are obviously different, and there is an obvious spin exchange between $|\psi_1|$ and $|\psi_{-1}|$ during the time evolution. However, in the deep unmagnetized phase [Figs. 7(a3)–7(d3)], $M = 0$, the wave packets of the two spin components $|\psi_1|$ and $|\psi_{-1}|$ almost coincide, and there is no spin exchange between $|\psi_1|$ and $|\psi_{-1}|$ in the time evolution.

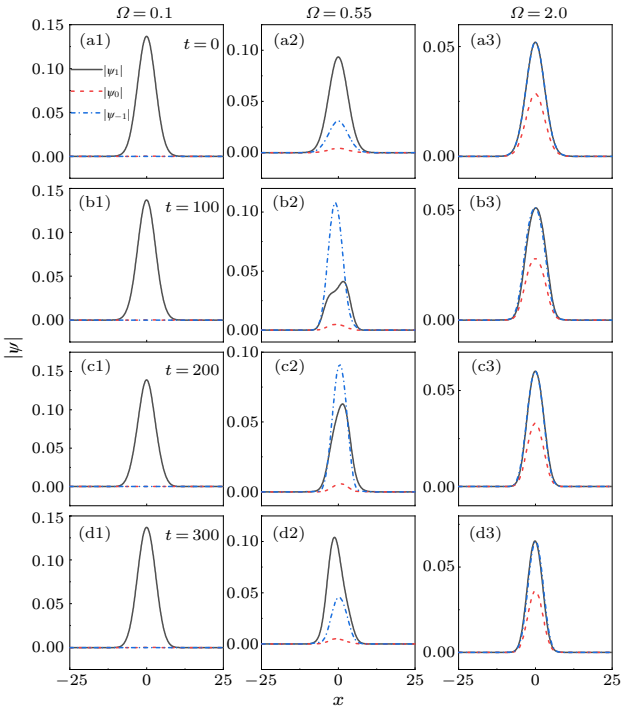



**Fig. 7.** Time evolutions of the three pseudo spin states $|\psi_1|$, $|\psi_0|$ and $|\psi_{-1}|$ in the fully magnetization phase with $\Omega = 0.1$ (the first column), in the magnetized phase near phase transition point with $\Omega = 0.55$ (the second column) and in the deep unmagnetized phase with $\Omega = 2.0$ (the third column). We set $g_0 = 1$, $g_2 = -0.5$, $\gamma = 0.1$, $\omega = 0.1$, and $\Delta = -4$.

## 6. Conclusions

In summary, we have characterized the collective excitations of interacting SO-coupled spin-1 BECs in harmonic potential. We analytically predict the dipolar and breather modes in collective excitations, which are well confirmed by the numerical results. The collective behaviors of the BECs can be regarded as the superposition of the multiple harmonic oscillations induced by the coupling effects of SO coupling, RC and atomic interactions. Therefore, the collective oscillations can translate between harmonic and anharmonic, which depends on the competition of the multiple external collective modes. In addition, the dipolar dynamics and breathing dynamics can be coupled due to the cooperative effect of spin momentum locking and spin-dependent interaction, and behaves distinct characters in different phases. Interestingly, in anharmonic oscillations, breathing oscillations can be induced by excited dipole oscillations, and vice versa. Our results provide theoretical evidence for identifying, exploring and manipulating the ground sate phases and collective dynamics of a system experimentally.

## Acknowledgments

This work was supported by the National Natural Science Foundation of China (Grant Nos. 12164042, 12264045,

11764039, 11475027, 11865014, 12104374, and 11847304), the Natural Science Foundation of Gansu Province (Grant Nos. 17JR5RA076 and 20JR5RA526), the Scientific Research Project of Gansu Higher Education (Grant No. 2016A-005), the Innovation Capability Enhancement Project of Gansu Higher Education (Grant Nos. 2020A-146 and 2019A-014), and the Creation of Science and Technology of Northwest Normal University (Grant No. NWNU-LKQN-18-33).

## Appendix A: The dimensional reduction of the model

The GPE describing the three-dimensional trapped SO-coupled spin-1 BECs can be written as

$$\begin{aligned}\mathrm{i}\hbar\frac{\partial\Psi}{\partial t}=&\Big[\frac{1}{2m}(p_x-2\hbar k_{\mathrm{R}}F_z)^2+\frac{1}{2}m\omega_x^2x^2+\sqrt{2}\tilde{\Omega}F_x+\tilde{\Delta}F_z^2\\&+g_0^{3\mathrm{D}}|\Psi|^2+g_2^{3\mathrm{D}}\Psi^{\dagger}\boldsymbol{F}^2\Psi\Big]\Psi\\&+\Big[\frac{p_\perp^2}{2m}+\frac{1}{2}m\omega_\perp^2(y^2+z^2)\Big]\Psi,\end{aligned}\tag{A1}$$

where $\Psi=(\psi_1,\psi_0,\psi_{-1})^{\mathrm{T}}$ is the spinor wave function, $p_x=-\mathrm{i}\hbar\partial_x$, $p_\perp=-\mathrm{i}\hbar(\partial_y+\partial_z)$, $g_0=4\pi\hbar^2(a_0+2a_2)/(3m)$, $g_2=4\pi\hbar^2(a_2-a_0)/(3m)$, $\tilde{\Omega}$ is the RC strength, and $\tilde{\Delta}$ is the quadratic Zeeman strength. We consider an SO coupling characterized by an equally weighted Rashba and Dresselhaus SO coupling. The SO coupling only exists in the $\hat{x}$ direction and mainly affects the collective dynamics in the $\hat{x}$ direction, while the dipole oscillations in the $\hat{y}$ and $\hat{z}$ directions are still harmonic oscillations, and the oscillation frequency is the harmonic potential frequency in that direction. Furthermore, when the strength of the trapping potential in the $\hat{y}$ and $\hat{z}$ directions is much larger than the frequency of the trapping potential in the $\hat{x}$ direction, the transverse degrees of freedom of the system are frozen such that the dynamics of the system only occurs in the $\hat{x}$ direction. Therefore, we consider the one-dimensional case and discuss the nonlinear mode coupling caused by SO coupling in the $\hat{x}$ direction. The three-dimensional wave function can be decomposed into

$$\Psi(\boldsymbol{r},t)=\Psi(\boldsymbol{x},t)\phi(y,z),\tag{A2}$$

where

$$\phi(y,z)=\frac{1}{\sqrt{\pi}l_\perp^2}\exp\Big[-\frac{y^2+z^2}{2l_\perp^2}\Big],\tag{A3}$$

$l_\perp=\sqrt{\hbar/(m\omega_\perp)}$. Then, substituting Eqs. (A2) and (A3) into Eq. (A1) and integrating over $(-\infty,\infty)$ for $x$ and $y$, one can obtain

$$\begin{aligned}\mathrm{i}\hbar\frac{\partial\Psi}{\partial t}=&\Big[\frac{1}{2m}(p_x-2\hbar k_{\mathrm{R}}F_z)^2+\frac{1}{2}m\omega_x^2x^2+\sqrt{2}\tilde{\Omega}F_x+\tilde{\Delta}F_z^2\\&+\frac{g_0^{3\mathrm{D}}}{2\pi l_\perp^2}|\Psi|^2+\frac{g_2^{3\mathrm{D}}}{2\pi l_\perp^2}\Psi^{\dagger}\boldsymbol{F}^2\Psi\Big]\Psi.\end{aligned}\tag{A4}$$

A constant is ignored in Eq. (A4). Comparing Eqs. (A4) with (A1), we can find that the dimensional reduction of the GPE only causes a correction for the strength of interactions.

For convenience, the variables are rescaled as $t\sim t\omega_\perp^{-1}$, $x\sim l_\perp x$ and $\Psi\sim\sqrt{N/l_\perp}\Psi$, then the dimensionless equation is

$$\begin{aligned}\mathrm{i}\frac{\partial\Psi}{\partial t}=&\Big[-\frac{1}{2}\partial_x^2+\mathrm{i}2\gamma\partial_xF_z+(\Delta+2\gamma^2)F_z^2+\sqrt{2}\Omega F_x\\&+\frac{1}{2}\omega^2x^2+g_0|\Psi|^2+g_2\Psi^{\dagger}\boldsymbol{F}^2\Psi\Big]\Psi,\end{aligned}\tag{A5}$$

where $g_0=2N\hbar(a_0+2a_2)/(3m\omega_\perp l_\perp^3)$, $g_2=2N\hbar(a_2-a_0)/(3m\omega_\perp l_\perp^3)$, $\gamma=l_\perp k_{\mathrm{R}}$, $\Omega=\tilde{\Omega}/(\hbar\omega_\perp)$, and $\Delta=\tilde{\Delta}/(\hbar\omega_\perp)$.

The obtained dimensionless parameters can be estimated according to the relevant experimental parameters.[7,34,39] Taking the wavelength of the Raman laser as $\lambda_{\mathrm{R}}=804.3$ nm, trapped potential frequency $\omega_x=2\pi\times20$ Hz and $\omega_y=\omega_z=2\pi\times400$ Hz and atomic number $N=10000$, then the oscillator lengths in the $\hat{x}$ direction and the transverse direction are $l_0=2.41$ μm and $l_\perp=0.571$ μm, respectively; SO coupling $\gamma\sim4$, RC strength $\Omega\sim0$–$100$ and quadratic Zeeman strength $|\Delta|\sim0$–$35$ are experimentally adjustable to a large extent. For $^{87}$Rb atoms, the scattering length $a_0=5.387$ nm and $a_2=5.313$ nm, then the reduced density-dependent interaction $g_0\sim200$ and spin-dependent interaction $g_2\sim-1$ can be obtained. However, for $^{23}$Na atoms, the scattering length $a_0=2.646$ nm and $a_2=2.919$ nm, then $g_0\sim53$ and $g_2\sim2$. Therefore, the physical parameters used in this paper are all within the ranges of experimental parameters.

## Appendix B: Linearization coefficients

The linearization coefficients mentioned in Section 3 are given as follows:

$$C_1=\frac{1}{R^4}+3\omega^2,\tag{B1}$$

$$C_2=\frac{2\sqrt{2}g_2M}{\sqrt{\pi}R^2\sqrt{m_z^2-M^2}}\Big(\sqrt{m_z^2-M^2}-1+m_z\Big),\tag{B2}$$

$$C_3=\frac{2\sqrt{2}g_2}{\sqrt{\pi}R^2}\Big(1-\sqrt{m_z^2-M^2}-2m_z-\frac{m_z(1+m_z)}{\sqrt{m_z^2-M^2}}\Big),\tag{B3}$$

$$a_{0,1}=\sqrt{2-2m_z}(\sqrt{m_z-M}\pm\sqrt{m_z+M}),\tag{B4}$$

$$a_2=\frac{2\sqrt{2}g_2(1-m_z)(M^2-m_z^2)}{\sqrt{\pi}R\sqrt{m_z^2-M^2}},\tag{B5}$$

$$a_3=\frac{g_2M}{\sqrt{2\pi}R^2}\Big(1-\frac{1-m_z}{\sqrt{m_z^2-M^2}}\Big),\tag{B6}$$

$$\begin{aligned}a_4=&-\frac{g_2}{\sqrt{2\pi}R^2}\Big(1-\frac{1-m_z}{\sqrt{m_z^2-M^2}}\Big)-\frac{\Omega\sqrt{1-m_z}}{2\sqrt{2}(m_z+M)^{3/2}}\\&-\frac{\Omega\sqrt{1-m_z}}{2\sqrt{2}(m_z-M)^{3/2}}-\frac{g_2M(1-m_z)}{2\sqrt{2\pi}R\sqrt{m_z-M}(m_z+M)^{3/2}}\\&-\frac{g_2M(1-m_z)}{2\sqrt{2\pi}R\sqrt{m_z+M}(m_z-M)^{3/2}},\end{aligned}\tag{B7}$$

$$a_5 = -\frac{\Omega\sqrt{1-m_z}}{2\sqrt{2}}\left(\frac{1}{(m_z+M)^{3/2}}-\frac{1}{(m_z-M)^{3/2}}\right) - \frac{\Omega\sqrt{1-m_z}}{2\sqrt{2}(m_z-1)}\left(\frac{1}{\sqrt{m_z-M}}-\frac{1}{\sqrt{m_z+M}}\right) - \frac{g_2M(1-m_z)}{2\sqrt{2\pi}R\sqrt{m_z^2-M^2}}\left(\frac{2}{(1-m_z)}+\frac{1}{m_z+M}+\frac{1}{m_z-M}\right), \tag{B8}$$

$$a_6 = \frac{g_2}{\sqrt{2\pi}R^2}\left(1+\frac{m_z(1-m_z)}{\sqrt{m_z^2-M^2}}-2m_z\right), \tag{B9}$$

$$a_7 = \frac{\sqrt{2}g_2}{\sqrt{\pi}R}+\frac{g_2(1-m_z)}{\sqrt{2\pi}R}\left(\frac{1}{m_z-M}+\frac{1}{m_z+M}\right) - \frac{\Omega\sqrt{1-m_z}}{2\sqrt{2}}\left(\frac{1}{(m_z+M)^{3/2}}+\frac{1}{(m_z-M)^{3/2}}\right) - \frac{\Omega}{2\sqrt{2}\sqrt{1-m_z}}\left(\frac{1}{\sqrt{m_z-M}}+\frac{1}{\sqrt{m_z+M}}\right) + \frac{\Omega\sqrt{1-m_z}}{2\sqrt{2}(m_z-1)}\left(\frac{1}{\sqrt{m_z-M}}+\frac{1}{\sqrt{m_z+M}}\right) + \frac{g_2(M^2+m_z-m_z^2)}{2\sqrt{2\pi}R\sqrt{m_z^2-M^2}}\left(\frac{1}{m_z+M}+\frac{1}{m_z-M}\right) + \frac{g_2m_z(m_z-1)}{\sqrt{2\pi}R(m_z^2-M^2)}+\frac{\Omega(\sqrt{m_z-M}+\sqrt{m_z+M})}{\sqrt{2\pi}R\sqrt{m_z^2-M^2}} - \frac{(1-m_z)\sqrt{1-m_z}}{2\sqrt{2}(1-m_z)}, \tag{B10}$$

$$a_8 = \frac{g_2(1/2-m_z)}{\sqrt{2\pi}R}\left(\frac{1}{m_z+M}-\frac{1}{m_z-M}\right) - \frac{\Omega\sqrt{1-m_z}}{2\sqrt{2}}\left(\frac{1}{(m_z-M)^{3/2}}-\frac{1}{(m_z+M)^{3/2}}\right) - \frac{\Omega}{2\sqrt{2}\sqrt{1-m_z}}\left(\frac{1}{\sqrt{m_z-M}}-\frac{1}{\sqrt{m_z+M}}\right) + \frac{\Omega\sqrt{1-m_z}}{2\sqrt{2}(m_z-1)}\left(\frac{1}{\sqrt{m_z-M}}+\frac{1}{\sqrt{m_z+M}}\right) + \frac{g_2(M^2+m_z-2m_z^2)}{2\sqrt{2\pi}R\sqrt{m_z-M}(m_z+M)^{3/2}} - \frac{g_2(M^2+m_z-2m_z^2)}{2\sqrt{2\pi}R\sqrt{m_z+M}(m_z-M)^{3/2}}-\frac{\Omega\sqrt{m_z-M}}{2\sqrt{2}(1-m_z)^{3/2}} + \frac{g_2M(1-m_z)}{\sqrt{2\pi}R(m_z^2-M^2)}-\frac{\sqrt{2}g_2M}{\sqrt{\pi}R\sqrt{m_z^2-M^2}} - \frac{\Omega\sqrt{m_z+M}}{2\sqrt{2}(1-m_z)^{3/2}}, \tag{B11}$$

where $M$, $m_z$ and $R$ are taken in the ground state and are determined by Eqs. (6)–(13).

## References


[1] Dalibard J, Gerbier F, Juzeliūnas G and Öhberg P 2011 *Rev. Mod. Phys.* **83** 1523

[2] Galitski V and Spielman I B 2013 *Nature* **494** 49

[3] Goldman N, Juzeliūnas G, Öhberg P and Spielman I B 2014 *Rep. Prog. Phys.* **77** 126401

[4] Qi R, Yu X L, Li Z B and Liu W M 2009 *Phys. Rev. Lett.* **102** 185301

[5] Lin Y J, Jimenez-Garcia K and Spielman I B 2011 *Nature* **471** 83

[6] Fu Z, Wang P, Chai S, Huang L and Zhang J 2011 *Phys. Rev. A* **84** 043609

[7] Zhang J Y, Ji S C, Chen Z, Zhang L, Du Z D, Yan B, Pan G S, Zhao B, Deng Y J, Zhai H, Chen S and Pan J W 2012 *Phys. Rev. Lett.* **109** 115301

[8] Wang P, Yu Z Q, Fu Z, Miao J, Huang L, Chai S, Zhai H and Zhang J 2012 *Phys. Rev. Lett.* **109** 095301

[9] Cheuk L W, Sommer A T, Hadzibabic Z, Yefsah T, Bakr W S and Zwierlein M W 2012 *Phys. Rev. Lett.* **109** 095302

[10] Qi X L and Zhang S C 2011 *Rev. Mod. Phys.* **83** 1057

[11] Martone G I, Pepe F V, Facchi P, Pascazio S and Stringari S 2016 *Phys. Rev. Lett.* **117** 125301

[12] Yu Z Q 2016 *Phys. Rev. A* **93** 033648

[13] Sun K, Qu C L, Xu Y, Zhang Y P and Zhang C W 2016 *Phys. Rev. A* **93** 023615

[14] Wen L, Sun Q, Wang H Q, Ji A C and Liu W M 2012 *Phys. Rev. A* **86** 043602

[15] Ji S C, Zhang L, Xu X T, Wu Z, Deng Y, Chen S and Pan J W 2015 *Phys. Rev. Lett.* **114** 105301

[16] Zheng W and Li Z B 2012 *Phys. Rev. A* **85** 053607

[17] Zhang Y P, Mao L and Zhang C W 2012 *Phys. Rev. Lett.* **108** 035302

[18] Li Y, Martone G I and Stringari S 2012 *Europhys. Lett.* **99** 56008

[19] Dalfovo F, Giorgini S, Pitaevskii L P and Stringari S 1999 *Rev. Mod. Phys.* **71** 463

[20] Stringari S 1996 *Phys. Rev. Lett.* **77** 2360

[21] Kohn W 1961 *Phys. Rev.* **123** 1242

[22] Dalfovo F, Minniti C and Pitaevskii L P 1997 *Phys. Rev. A* **56** 4855

[23] Hechenblaikner G, Marag'o O M, Hodby E, Arlt J, Hopkins S and Foot C J 2000 *Phys. Rev. Lett.* **85** 692

[24] Hechenblaikner G, Morgan S A, Hodby E, Maragò O M and Foot C J 2002 *Phys. Rev. A* **65** 033612

[25] Huang G X, Li X Q and Szeftel J 2004 *Phys. Rev. A* **69** 065601

[26] Pitaevskii L and Stringari S 1997 *Phys. Lett. A* **235** 398

[27] Stamper-Kurn D M, Miesner H J, Inouye S, Andrews M R and Ketterle W 1998 *Phys. Rev. Lett.* **81** 500

[28] Pitaevskii L 1997 *Phys. Lett. A* **229** 406

[29] Graham R, Walls D F, Collett M J, Fliesser M and Wright E M 1998 *Phys. Rev. A* **57** 503

[30] Chen Y Y, Lyu H, Xu Y and Zhang Y P 2022 *New J. Phys.* **24** 073041

[31] Chen Z and Zhai H 2012 *Phys. Rev. A* **86** 041604

[32] Rajat, Roy A and Gautam S 2022 *Phys. Rev. A* **106** 013304

[33] Zhang W X, Zhou D L, Chang M S, Chapman M S and You L 2005 *Phys. Rev. A* **72** 013602

[34] Campbell D L, Price R M, Putra A, Valds-Curiel A, Trypogeorgos D and Spielman I B 2016 *Nat. Commun.* **7** 10897

[35] Lin Y J, Compton R L, Perry A R, Phillips W D, Porto J V and Spielman I B 2009 *Phys. Rev. Lett.* **102** 130401

[36] Sun J, Chen Y Y, Chen X and Zhang Y P 2020 *Phys. Rev. A* **101** 053621

[37] Boninsegni M and Prokofev N V 2012 *Rev. Mod. Phys.* **84** 759

[38] Ho T L 1998 *Phys. Rev. Lett.* **81** 742

[39] Gautam S and Adhikari S K 2014 *Phys. Rev. A* **90** 043619

[40] Ohmi T and Machida K 1998 *J. Phys. Soc. Jpn.* **67** 1822

[41] Stamper-Kurn D M and Ueda M 2013 *Rev. Mod. Phys.* **85** 1191

[42] Chin C, Grimm R, Julienne P and Tiesinga E 2010 *Rev. Mod. Phys.* **82** 1225

[43] Pérez-García V M, Michinel H, Cirac J I, Lewenstein M and Zoller P 1996 *Phys. Rev. Lett.* **77** 5320

[44] Pérez-García V M, Michinel H, Cirac J I, Lewenstein M and Zoller P 1997 *Phys. Rev. A* **56** 1424